CHEMISTRY
A EUROPEAN JOURNAL

DOI: 10.1002/chem.200700837

Contrasting Photodynamics between C_{60}–Dithiapyrene and C_{60}–Pyrene Dyads

Dirk M. Guldi,*[a] Fabian Spänig,[a] David Kreher,[b] Igor F. Perepichka,[b, d] Cornelia van der Pol,[b] Martin R. Bryce,*[b] Kei Ohkubo,[c] and Shunichi Fukuzumi*[c]

Dedicated to the memory of Janos H. Fendler

Abstract: The photodynamics of a C_{60}–dithiapyrene donor–acceptor conjugate were compared with the corresponding C_{60}–pyrene conjugate. The photoinduced charge separation and subsequent charge recombination processes were examined by time-resolved fluorescence measurements on the picosecond timescale and transient absorption measurements on the picosecond and microsecond timescales with detection in the visible and near-infrared regions. We have observed quite long lifetimes (i.e., up to 1.01 ns) for the photogenerated charge-separated state in a C_{60}–dithiapyrene dyad without the need for i) a long spacer between the two moieties, or ii) a gain in aromaticity in the radical ion pair.

Keywords: dyads · electron transfer · fullerenes · photodynamics · pyrenes

Introduction

Covalently linked donor–acceptor conjugates including fullerene C_{60} have attracted much attention because electron-transfer reactions to C_{60} are highly efficient due to the minimal changes of structure and solvation that are associated with the electron-transfer reduction.[1–5] Such conjugates have been widely used in photoelectronic devices such as photovoltaic cells.[6,7] As electron donors for linkage to C_{60}, porphyrins have frequently been used, because porphyrins, which contain an extensively conjugated two-dimensional π-system, are also suitable for efficient electron transfer due to the minimal structural and solvation changes upon electron transfer. In addition, rich and extensive absorption features of porphyrinoid systems guarantee increased absorption cross-sections and an efficient use of the solar spectrum.[8–10] However, only polar solvents can be used for charge separation, since the charge-separated state cannot be observed in non-polar solvents where the charge separation energy exceeds that of the triplet energy of C_{60}. In such a case the photoexcitation of the donor–acceptor conjugates leads to the formation of the triplet excited state of C_{60} rather than the radical ion pair state.[11] As compared to porphyrins, tetrathiafulvalene (TTF) provides an important advantage due to the stabilization of the radical ion pair state of the C_{60} conjugates relative to the triplet excited state of the C_{60} moiety.[5,12–16] 1,6-Dithiapyrene (DTP, **1**) is also known to act as an excellent Weitz-type electron donor with a reduction potential comparable to that of TTF.[17,18] A key difference between DTP (**1**) and TTF is that DTP is aromat-

[a] Prof. D. M. Guldi, F. Spänig
Institute for Physical Chemistry
Friedrich-Alexander-Universität Erlangen-Nürnberg
Egerlandstrasse 3, 91058 Erlangen (Germany)
Fax: (+49) 9131-852-8307
E-mail: dirk.guldi@chemie.uni-erlangen.de

[b] Dr. D. Kreher, Dr. I. F. Perepichka, C. van der Pol, Prof. M. R. Bryce
Department of Chemistry and Centre for Molecular and Nanoscale Electronics, Durham University
Durham DH1 3LE (UK)
Fax: (+44) 191-384-4737
E-mail: m.r.bryce@durham.ac.uk

[c] Dr. K. Ohkubo, Prof. S. Fukuzumi
Department of Material and Life Science
Graduate School of Engineering, Osaka University
SORST, JAPAN Science and Technology Agency
Suita, Osaka 565-0871 (Japan)
E-mail: fukuzumi@ap.chem.eng.osaka-u.ac.jp

[d] Dr. I. F. Perepichka
On leave from:
National Academy of Sciences of Ukraine
L. M. Litvinenko Institute of Physical Organic and Coal Chemistry
Donetsk 83114 (Ukraine)

Supporting information for this article is available on the WWW under http://www.chemeurj.org/ or from the author: Synthetic procedures for compounds **1**–**3**, Figures S1–S33, comprising 1D and 2D NMR spectroscopic data, cyclic voltammetry data, electronic absorption and differential absorption spectra, DFT calculations including orbital energy levels diagrams, orbital localization and tables of optimized geometries.

ic (18 π-electrons) in the neutral state, whereas TTF has a non-aromatic neutral state (two 7 π-electron rings) and gains aromaticity (formation of 6 π-electron dithiolium cations) upon oxidation. 1,6-Dithiapyrene (**1**) has more extensive absorption in the visible region, acting as a better chromophore than TTF. However, donor–acceptor dyads composed of dithiapyrene and C_{60} have yet to be reported, despite the evident interest in combining these moieties.

We report herein the synthesis and photodynamics of C_{60}–dithiapyrene conjugate **4**. The corresponding C_{60}–pyrene conjugate **6** with virtually the same geometry was synthesized to compare the photodynamics between C_{60}–dithiapyrene and C_{60}–pyrene dyads. In order to confirm the photoinduced charge separation and subsequent charge-recombination processes, we employed time-resolved fluorescence measurements on the picosecond timescale and transient absorption measurements on the pico- and microsecond timescale with detections that range from the visible to the near-infrared regions. The present study provides deeper insight into the control of the electron-transfer processes by subtle changes in the redox potentials and/or solvent polarity.

Results and Discussion

Synthesis: Functionalization of **1** is essentially unexplored[17–21] and no **1**–acceptor dyads have been reported. Derivatives of **1** functionalized only at positions 2 and 7 are known from the literature, which are accessible through lithiation chemistry [reaction with *n*BuLi followed by quenching with an electrophile, for example, $C_6F_{13}I$[19] or *N*,*N*-dimethylformamide (DMF)[20] resulting in 2-iodo-, 2,7-diodo- or 2-formyl-derivatives, respectively]. We have found that electrophilic substitution in **1** opens an access to 1,6-dithiapyrenes functionalized at position 5: reaction of **1** with phosphorus oxychloride and DMF under Vilsmeier conditions gave 5-formyl derivative **2** in 68% yield.

The new 5-formyl derivative **2** has a melting point range of 255–257 °C, which is substantially different from the known 2-formyl-1,6-dithiapyrene (m.p. 215–216 °C).[20] Considering that other physical data for these two isomers are similar (e.g. elemental analyses, MS, number of signals in ^{1}H and ^{13}C NMR, and splitting in ^{1}H NMR spectra) and routine one-dimensional NMR spectroscopy did not confirm the position of functionalization in the 1,6-dithiapyrene ring, the structure of **2** was proved by 2D-NMR spectroscopy studies (COSY, NOESY techniques, see Supporting Information Figures S1–S9). In order to provide further confirmation of this structure, aldehyde **2** was converted into the aldimine **3** (see Supporting Information). The increased solubility introduced by the cyclohexyl moiety of **3** enabled more detailed NMR spectroscopic studies (COSY, NOESY, HSQC, HMBC techniques) to be preformed to unambiguously assign the structure (Supporting Information, Figures S10–S15).

Reaction of **2** with C_{60} via Prato's 1,3-dipolar cycloaddition protocol with an azomethine ylide generated in situ[22] afforded the mono-adduct **4** (64% yield) (Scheme 1). A similar Prato reaction of pyrene-1-carboxaldehyde (**5**) gave C_{60}–pyrene dyad **6** in 56% yield. Although electrochemical investigations on dyad **6** have been reported recently,[23] no details on its synthesis and characterization have been given. Both structures were assigned from ^{1}H NMR spectra, MALDI-TOF MS and electronic absorption spectra. Dyad **6** was additionally characterized by ^{13}C NMR spectroscopy (solubility of dyad **4** is very low for ^{13}C NMR, but it showed satisfactory elemental analyses).

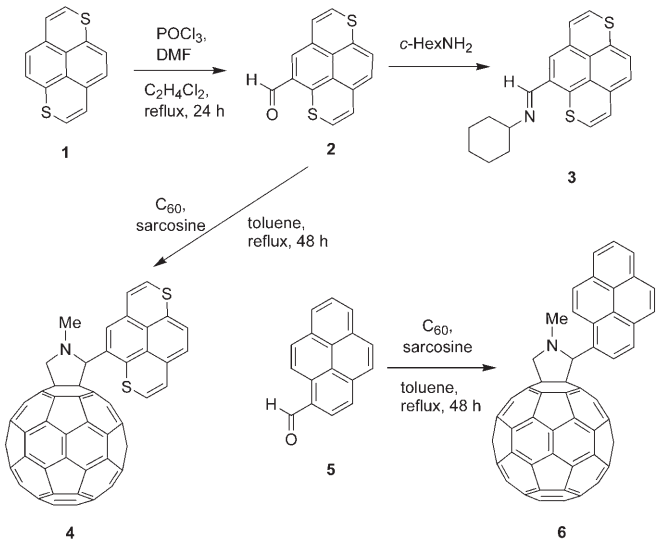

Scheme 1. Synthesis of the compounds discussed herein.

Theoretical calculations: Prior to the photophysical investigations we tested the donor and acceptor features in C_{60}–dithiapyrene (**4**) and C_{60}–pyrene (**6**). In this context, B3LYP/6-31G(d) calculations emerged as an important reference point. They reveal that in fully optimized geometries the HOMO and LUMO are exclusively delocalized over the dithiapyrene (−4.58 eV)/pyrene (−5.39 eV) and C_{60} (−3.05/−3.06 eV) moieties, respectively (Figure 1; for more details on DFT calculations see Figures S30–S33 in Supporting Information). This reflects a lack of electronic interactions between the donor and acceptor fragments in both donor–acceptors systems, despite imminent close center-to-center distances between the donor and the acceptor moieties of 8.17 and 8.30 Å in **4** and **6**, respectively. The small effects of the donor units on the LUMO (0.17–0.18 eV) and the acceptor unit on the HOMO energy levels (0.14 eV) in C_{60}–dithiapyrene (**4**) and C_{60}–pyrene (**6**)—as evidenced from comparison with parent DTP (**1**) and C_{60}, Figure 2—are in good agreement with the lack of electronic interactions between the donor and acceptor moieties. Considering the energies of the two HOMO and LUMO levels we estimate energy gaps in the gas phase of 1.53 eV for C_{60}–dithiapyrene and 2.34 eV for C_{60}–pyrene (Figure 2).

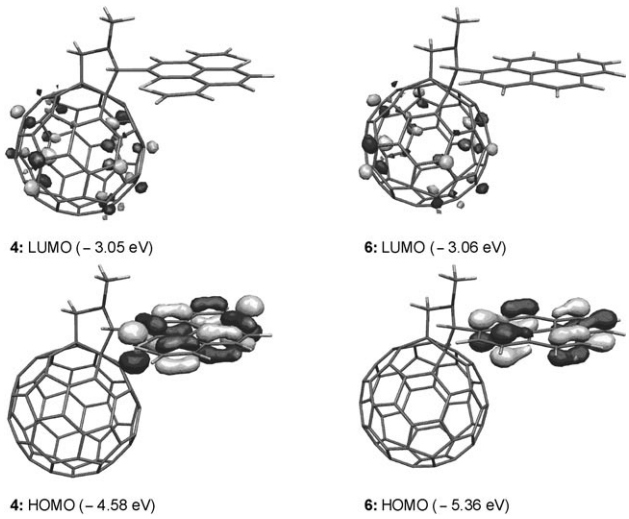

Figure 1. Localization of HOMO and LUMO orbitals in dyads **4** and **6** according to B3LYP/6-31G(d) calculations.

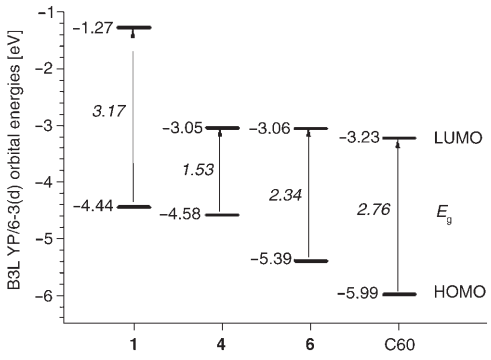

Figure 2. Energy levels of frontier orbitals of dyads **4** and **6** in comparison with those for DTP (**1**) and C_{60} from DFT B3LYP/6-31G(d) calculations in the gas phase.

Electrochemistry: The solution redox properties of C_{60}–dithiapyrene (**4**) and C_{60}–pyrene (**6**) were studied by cyclic voltammetry (CV) along with compounds **1**, C_{60} and the model *N*-methylfulleropyrrolidine (**7**; Table 1). Compound **1** displayed two reversible, one-electron oxidation waves at low potentials, due to sequential cation radical and dication formation, as described previously.[18] C_{60}–dithiapyrene (**4**), on the other hand, is highly redox amphoteric, displaying two single-electron oxidation waves from the DTP moiety and two single-electron reduction waves from the fullerene moiety (Figure 3, Table 1 and Figures S18–S22 in Supporting Information). Small donor–acceptor interactions in **4** result in slightly anodic shifts of the oxidation potentials of the DTP moiety compared to **1** (by 0.07 V for $E_{1ox}^{1/2}$ and 0.02 V for $E_{2ox}^{1/2}$) and little cathodic shifts of the reduction potentials of the C_{60} moiety compared with **7** (by 0.02 V for both $E_{1red}^{1/2}$ and $E_{2red}^{1/2}$ in PhCN, Table 1). These results are in good agreement with theoretical predictions from DFT calculations discussed above for the evolution of HOMO–LUMO energies in **4** compared with **1** and C_{60}. A contribution to the cathodic shift of $E_{1red}^{1/2}$ in **4** compared with pristine C_{60} arises from breaking of a C=C double bond in the C_{60} system; thus, **7** showed a 90 mV cathodic shift of $E_{1red}^{1/2}$ compared with C_{60} (Table 1; cf. ref.[24]).

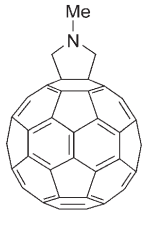

7

Reduction of C_{60}–pyrene (**6**) occurs at almost the same potentials as for **4** and **7** thus confirming a negligible effect of the donor units on the LUMO energy level. In contrast, the oxidation of the pyrene unit in **6** is anodically shifted by 0.91 V (from comparison of their E_{1ox}^{pa} potentials) compared with the oxidation of the DTP moiety in **4** and the process is electrochemically irreversible (Figure 3, Table 1).

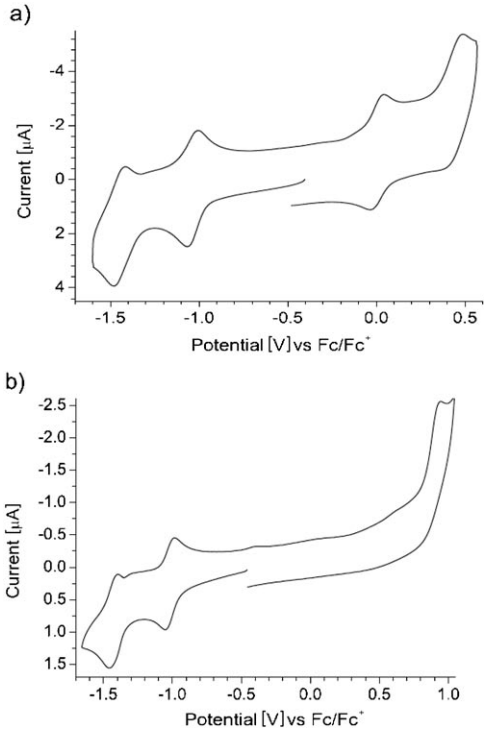

Figure 3. Cyclic voltammograms of a) C_{60}–dithiapyrene **4** (scan rate 500 mV s^{-1}) and b) C_{60}–pyrene **6** (scan rate 100 mV s^{-1}) dyads in benzonitrile, 0.1 M Bu_4NPF_6.

Photophysics: Orbital analysis of **4** confirms the expected localization of the HOMO on the dithiapyrene fragment and the LUMO on the C_{60} moiety (Figure 1). There is little orbital interaction between the donor and acceptor moieties as indicated by the electrochemical measurements (see above). This is also confirmed by the UV-visible spectrum, which is the superposition of that of each component as shown in Figure 4 (see also Figures S25 and S26 in the Supporting Information), in which the spectrum of C_{60}–pyrene **6** is given for comparison.

Table 1. Cyclic voltammetric data[a] for compounds **1**, **4**, **6**, **7**, and C_{60}.

Comp.	$E_{1ox}^{1/2}$ [V]	$E_{2ox}^{1/2}$ [V]	$E_{1red}^{1/2}$ [V]	$E_{2red}^{1/2}$ [V]	$E_{3red}^{1/2}$ [V]	E_g^{CV} [eV][b]
1[c]	−0.06	+0.41				
1[d]	−0.11	+0.39				
C_{60}[c]			−0.92	−1.33		
C_{60}[d]			−0.97	−1.38	−1.62	
4[c]	+0.01	+0.45[e]	−1.03	−1.45		0.87
6[c]	+0.95[e]		−1.02	−1.43	−1.82[f]	1.62
7[c]			−1.01	−1.43		

[a] Electrolyte 0.1 M Bu_4NPF_6; scan rate 100 mV s^{-1} (for **1**, **6** and C_{60}) and 500 mV s^{-1} (for **4**); potentials measured *vs.* Ag/Ag$^+$ reference electrode and standardized to Fc/Fc$^+$ couple [$E_{Fc/Fc}^{+} = +0.20$ V *vs.* Ag/Ag$^+$ (PhCN); +0.24 V (PhCN/*o*-DCB, 1:1 v/v)]. [b] HOMO–LUMO gap, estimated from the onsets of oxidation and reduction processes in CV. [c] CV in benzonitrile; see also ref. [23] for CV with the microcell in toluene/DMF 3:2. [d] CV in benzonitrile/*o*-DCB 1:1 v/v. [e] Irreversible peak (E_{1ox}^{pa}). [f] Irreversible peak (E_{1red}^{pc}).

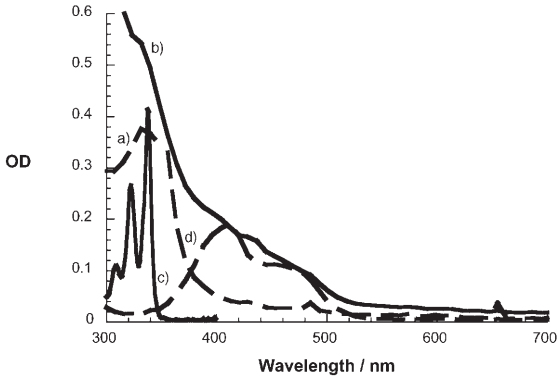

Figure 4. UV/Vis spectra of a) dithiapyrene, b) C_{60}–dithiapyrene **4**, c) pyrene and d) C_{60}–pyrene **6** in toluene.

Preliminary insights into conceivable donor–acceptor implications were gained from steady-state fluorescence experiments (Figure 5). Hereby, the fluorescing features of pyrene and dithiapyrene are particularly useful, since they enable the deactivation of the pyrene (3.22 eV) and dithiapyrene (2.43 eV) singlet excited states in the references, as well as in C_{60}–dithiapyrene **4** and in C_{60}–pyrene **6**, to be followed with ease. Specifically, fluorescence quantum yields of close to unity and fluorescence lifetimes of the order of tens of nanoseconds are sensitive markers. Notably, both sets of systems, that is, C_{60}–dithiapyrene **4** and C_{60}–pyrene **6**, exhibit dual fluorescence. Besides the strong fluorescence of dithiapyrene and pyrene in the visible part of the spectrum, C_{60} derivatives exhibit weak fluorescence in the near-infrared part of the spectrum (650–850 nm). In fact, the C_{60}-reference compound **7** (1.78 eV) reveals nearly solvent-independent fluorescence quantum yields of 6.0×10^{-4} and fluorescence lifetimes of 1.5 ns.

Relative to the strong fluorescence of the reference (0.75), the pyrene fluorescence in C_{60}–pyrene is nearly quantitatively quenched. Notably, the quenching is stronger in THF (i.e., 0.003) than in toluene (i.e., 0.005). Instead, the familiar fullerene fluorescence spectrum was found with a

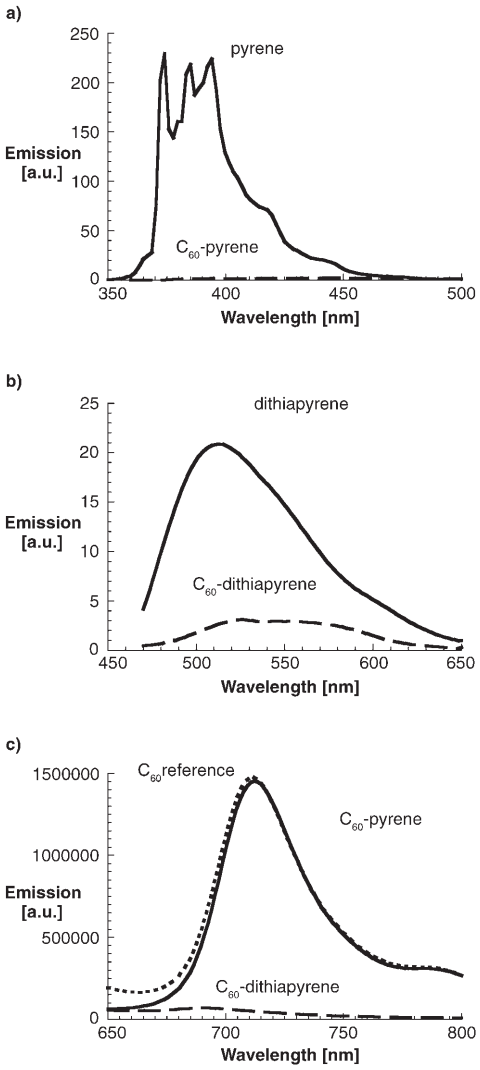

Figure 5. a) Fluorescence spectra in toluene with matching absorption at the a) 335 nm excitation; b) 460 nm excitation; and c) 325 nm excitation.

characteristic *0–0 transition around 715 nm, despite exclusive excitation of the pyrene moiety. To unravel the mechanism of producing the C_{60} fluorescence, an excitation spectrum was taken. The excitation spectrum of C_{60}–pyrene was an exact match of the ground state absorption of the fullerene reference **7** with maxima at 360 and 412 nm, respectively. This implies that there is a rapid transfer of singlet excited state energy from the photoexcited pyrene to the covalently linked C_{60}. Determining the quantum yield (6.0×10^{-4}) of the C_{60} fluorescence shows that its formation is quantitative, despite the exclusive excitation of the pyrene fragment.

Like in C_{60}–pyrene **6**, the dithiapyrene fluorescence (i.e., 0.023) in C_{60}–dithiapyrene **4** is subject to a marked fluorescence quenching that intensifies with the solvent polarity (e.g., toluene: 0.003; THF: 0.002). However, for C_{60}–dithiapyrene **4** no particular C_{60} fluorescence (i.e., $\ll10^{-5}$) was seen in the near-infrared region at all.

To complement the fluorescence studies, the photophysics of C_{60}–dithiapyrene **4** and C_{60}–pyrene **6** were probed by

means of time-resolved transient absorption spectroscopy. Femtosecond laser flash photolysis allowed for the characterization of the dynamic processes, which are associated with the generation and the fate of photoexcited states in these novel donor–acceptor conjugates, but more importantly, these data helped to shed light on the nature of the photoproduct, that is, an excited state or charge-separated state evolving from an intramolecular energy or electron transfer process, respectively.

First, the reference compounds should be discussed. In femtosecond-resolved transient absorption measurements, the pyrene reference gave rise to an instantaneously formed (i.e., within ≈ 2 ps), broadly absorbing transient with a maximum around 475 nm (Figure S27 in Supporting Information). On the timescale of up to 3000 ps no significant decay of the excited state absorption was observed. It is only on the hundreds of nanosecond timescale that the pyrene singlet excited state converts slowly (i.e., $4.3\times10^{6}\,s^{-1}$) to the corresponding triplet manifold, for which the following features were determined in our experiments: a transient maximum at 430 nm.

Similarly, dithiapyrene reveals on the femtosecond timescale the rapid formation (i.e., within ≈ 2 ps) of a singlet excited state, for which a maximum evolves at 530 nm (Figure S28 in Supporting Information). This state is metastable and another process follows, whose outcome on a timescale of 1500 ps is the formation of a distinct, new species, which is characterized by bleaching around 475 nm and a set of maxima at 515 and 550 nm. This absorption is in excellent agreement with that found upon nanosecond excitation, from which we infer that the underlying reaction is an intersystem crossing (i.e., $2.3\times10^{9}\,s^{-1}$) from the dithiapyrene singlet to the energetically lower lying triplet excited state. The triplet decays (i.e., $3.6\times10^{5}\,s^{-1}$) to the ground state.

Lastly, C_{60}-reference compound **7** should be discussed (Figure S29 in Supporting Information). The singlet excited state of compound **7** displays a distinctive singlet–singlet transition around 880 nm. The lifetime of the singlet–singlet intermediate state is relatively short, as C_{60} and most of its derivatives convert rapidly to the much longer-lived triplet excited state with nearly unit yield. The process is a spin-forbidden intersystem crossing (ISC) with a high rate of $5.0\times10^{8}\,s^{-1}$ driven by an efficient spin-orbit coupling. The spectral characteristics of the triplet excited state are maxima at 360 and 700 nm, followed by a low-energy shoulder at 800 nm.[25]

In the context of the current investigations, important features of the electron donors (i.e., dithiapyrene and pyrene) and the electron acceptor (i.e., C_{60}) are their corresponding radical cation and radical anion spectra, respectively. Thus, we have employed radiation chemical means to determine the spectral characteristics of the dithiapyrene radical cation, the pyrene radical cation and the fullerene radical anion. The following peaks evolve for the pyrene radical cation: 450, 500 and 575 nm.[26] For the dithiapyrene radical cation, on the other hand, peaks were noted at 560, 630 and 770 nm.

Following the conclusion of the femtosecond excitation (i.e., 355 nm) of C_{60}–pyrene **6** a transient intermediate is seen that—at first glance—resembles mostly that of the C_{60} reference. As Figure 6 shows the same broad maximum

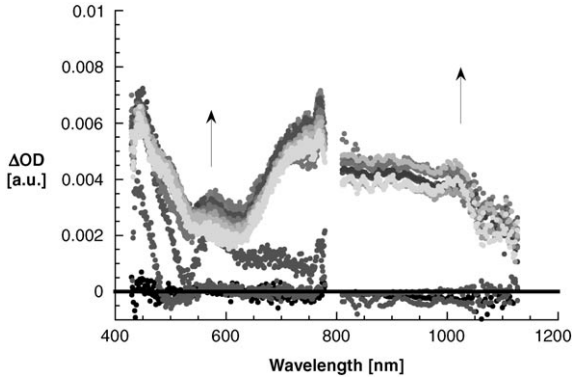

Figure 6. Differential absorption spectra (visible and near-infrared) obtained upon femtosecond laser flash photolysis (355 nm) of $\approx 1.0\times10^{-5}$ M solutions of C_{60}–pyrene **6** in deaerated THF at different delay times; excitation at 380 nm with OD = 0.6.

around 880 nm, which is indicative of the C_{60} singlet excited state, is seen regardless of the solvent (i.e., toluene and THF). This singlet excited state decays over the time course of 3000 ps and concomitant with this decay a maximum at 700 nm grows in. The latter is a clear attribute of the C_{60} triplet excited state. A closer inspection reveals, however, features that the C_{60} reference does not exhibit: maxima in the visible at 450, 510 and 575 nm and in the near-infrared at 1010 nm. Upon referral to the pulse radiolytic section we conclude that the 450, 510 and 575 nm features correspond to the pyrene radical cation, while the 1010 nm feature relates to the C_{60} radical anion. Hence, we see besides singlet and triplet excited states, the formation of an intermediate radical ion pair state.

Considering the aforementioned analysis of the spectral evolution it is hardly surprising that the best global fit of the absorption time profiles comprise a bi-exponential fitting function. In particular, in both solvents, namely toluene and THF, a short-lived and a long-lived component were found. Interestingly, the relative weight of the two contributions changes with solvent polarity. While, for example, in toluene the short-lived contribution is on the order of 5% it is nearly 50% in THF. The short lived component changes only slightly in the two solvents with values of 46 ± 6 ps and 53 ± 9 ps in toluene and THF, respectively. Contrasting these results the long-lived component is solvent independent and, more importantly, resembles the kinetics seen in the C_{60}-reference **7**. This leads us to conclude that the short-lived component must reflect the charge recombination, while the long-lived component is the intrinsic intersystem crossing affording the triplet excited state (see above). From such dependence we must assume that the charge recombination dynamics in C_{60}–pyrene **6** are located in the normal region of the Marcus parabola.

The behavior for C_{60}–dithiapyrene **4** is very different. Most importantly, with the help of spectroscopic and kinetic analysis we identified only one photoproduct. Immediately upon 380 nm photoexcitation the dithiapyrene singlet excited state features evolve, which attest to the successful dithiapyrene excitation despite the presence of C_{60}. C_{60} exerts, nevertheless, a profound impact on the singlet excited state decay. In particular, a rapid conversion (1.3×10^{12} s^{-1}) into a new transient is registered. Once the rapid disappearance of the excited dithiapyrene absorption comes to an end (i.e., $\approx$1.0 ps after the laser pulse), the following characteristics remain: maxima at 560, 630, 770 and 1010 nm, see Figure 7. The visible maxima are ascribed to the radical cation of dithiapyrene, because the dithiapyrene radical cation, produced by the one-electron oxidation of dithiapyrene **1** has

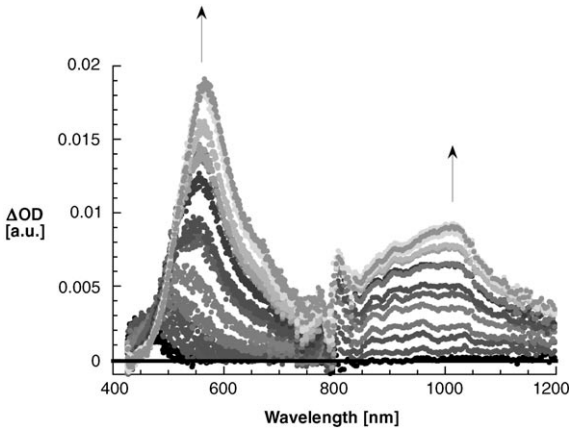

Figure 7. Differential absorption spectra (visible and near-infrared) obtained upon femtosecond laser flash photolysis (380 nm) of $\approx1.0\times10^{-5}$ M solutions of C_{60}–dithiapyrene **4** in deaerated toluene at different delay times; excitation at 380 nm with OD = 0.4.

absorption bands at 560, 630 and 770 nm. The absorption maximum in the near-infrared region, on the other hand, is an excellent match to the one-electron reduced fullerene. We therefore conclude that photoexcitation of C_{60}–dithiapyrene **4** yields in THF a radical ion pair state that evolves from the dithiapyrene and/or C_{60} singlet excited state. A similar radical ion pair state is also obtained in cyclohexane, toluene and DMF. Please note that no C_{60} singlet excited state features are discernable, neither in toluene nor THF, at any given time delay after the photoexcitation. On this basis we rule out any significant contribution that might evolve from a transduction of singlet excited state energy between DTP (**1**) (2.43 eV) and C_{60} (1.78 eV). The time profiles of the absorbance at 670 nm and 1014 nm in THF and toluene are shown in Figure 8. The lifetimes are determined as $\tau_{CS}=0.5$ ps (2.0×10^{12} s^{-1}) in DMF, $\tau_{CS}=2$ ps (5.0×10^{11} s^{-1}) in THF, $\tau_{CS}=27$ ps (3.9×10^{10} s^{-1}) in toluene and $\tau_{CS}=$ 1011 ps (9.8×10^{8} s^{-1}) in cyclohexane.

The slower charge-recombination rate in toluene than that in a more polar solvent (THF) suggests that this process is in the Marcus inverted region, where the electron-transfer rate becomes slower with increasing the driving force of electron transfer as the solvent polarity decreases.[27] This is demonstrated in Figure 9, which displays the driving force dependence ($-\Delta G^{o}$) for the charge recombination on the rate constant for both donor–acceptor conjugates (i.e., C_{60}–dithiapyrene **4** and C_{60}–pyrene **6**), see the Supporting Information for details. The parabolic fitting affords a reorganization energy (λ) of 0.89 eV and an electronic coupling (V) of 32 cm^{-1}. Both of these values are well in line with recently published donor–acceptor conjugates including fullerene C_{60}.[1–6]

In the corresponding nanosecond experiments C_{60}–dithiapyrene **4** and C_{60}–pyrene **6** give rise to contrasting behavior. While in the former case no appreciable changes were monitored on the nanosecond scale at all, in the latter case triplet characteristics were found that resemble those of the C_{60} reference. A high triplet quantum yield—with a value of 0.75 ± 0.05 in toluene and THF—corroborates the efficiency of the overall energy transfer. At the same time it points to the competition between energy and electron transfer when photoexciting pyrene. The triplets in the C_{60} reference and in the C_{60}–pyrene donor–acceptor conjugate **6** decay similarly slow on a time scale of up 100 microseconds to afford quantitatively the singlet ground state.

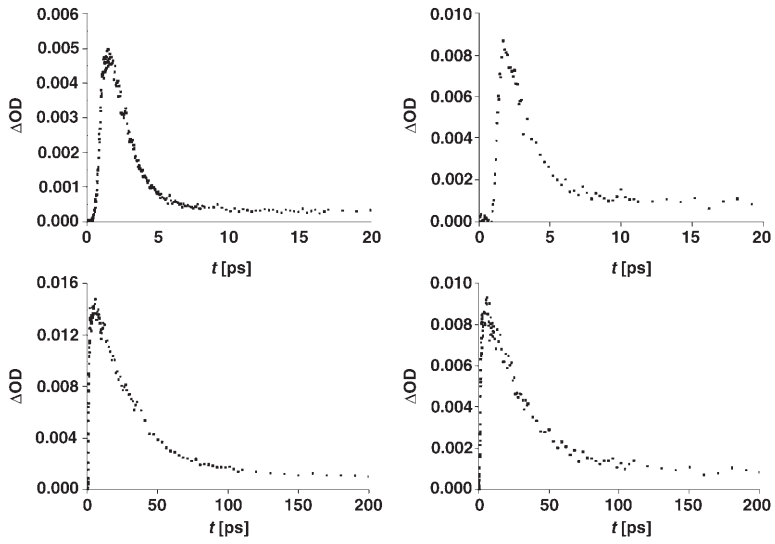

Figure 8. Time profiles of the transient absorption at 670 (left side) and 1014 (right side) nm monitoring the charge separation and recombination in C_{60}–dithiapyrene dyad **4**. Upper part in THF and lower part in toluene.

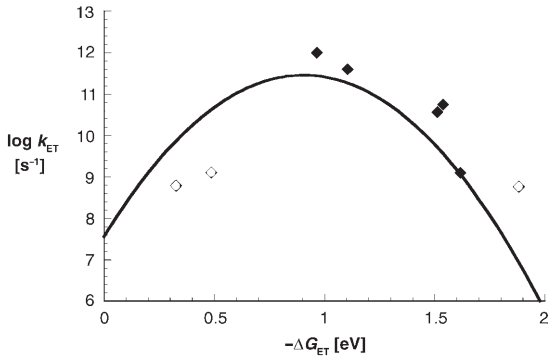

Figure 9. Driving force ($-\Delta G^{o}$) dependence of intramolecular charge recombination in C_{60}–dithiapyrene **4** (◆) and C_{60}–pyrene **6** (◇).

Conclusion

In summary, we have observed quite long lifetimes (i.e., up to 1.01 ns) for the photogenerated charge-separated state in a C_{60}–dithiapyrene **4** dyad without the need for i) a long spacer between the two moieties, or ii) a gain in aromaticity in the radical ion pair. This unexpected result raises issues of topology and aromaticity, which challenge the current views on designing C_{60} derivatives with long lifetimes for charge-separated species.

Experimental Section

Materials: Fullerene (C_{60}) was purchased from MER Corporation Nanotubes (Tuscon, USA). All other materials and solvents used for the synthesis of these compounds were purchased from Aldrich, Alfa Aesar, Merck or Acros and used as received. Compound **7** was obtained as described previously.[28] Photophysical measurements used C_{60} purchased from Kaesdorf (Geräte für Forschung und Industrie, München, Germany) and Science Laboratories Co., Ltd., Japan, and used as received. Solvents were purchased from Wako Pure Chemical Ind. Ltd., Japan, and purified according to the standard procedure.[29]

1,6-Dithiapyrene-5-carboxaldehyde (2): Phosphorus oxychloride (160 μL, 1.72 mmol) was added slowly to a solution of **1**[18] (280 mg, 1.17 mmol) and DMF (144 μL, 1.86 mmol) in 1,2-dichloroethane (20 mL) cooled in an ice bath. This mixture was stirred at reflux 24 h. After cooling, the reaction mixture was poured into ice-water and neutralized to pH 7 with 10% NaOH solution. The solution was extracted with CH_2Cl_2, and the organic phase was dried over $MgSO_4$ and evaporated. The residue was chromatographed (alumina, CH_2Cl_2/petrol ether 1:1) to afford compound **2** (220 mg, 68%) as black-violet solid. M.p. 255–257 °C; ^{1}H NMR (400 MHz, $CDCl_3$ + trace Et_3N): δ = 9.70 (s, 1H), 6.56 (d, J=7.7 Hz, 1H), 6.45 (s, 1H), 6.38 (d, J=7.7 Hz, 1H), 6.19 (d, J=9.9 Hz, 1H), 5.98 (d, J=10.1 Hz, 1H), 5.82 (d, J=10.3 Hz, 1H), 5.63 ppm (d, J=10.3 Hz, 1H); ^{13}C NMR (125 MHz, $CDCl_3$ + trace Et_3N): δ 189.0, 139.4, 134.9, 133.2, 131.6, 130.5, 129.7, 126.7, 126.0, 125.7, 124.9, 124.51, 124.48, 121.42, 120.9 ppm; EI: m/z (%): 268 (100) $[M]^+$; UV/Vis (CH_2Cl_2): λ_{max} = 328, 392, 412, 554, 582 nm; elemental analysis calcd (%) for $C_{15}H_8OS_2$ (268.35): C 67.14, H 3.00, S 23.90; found C 67.10, H 3.02, S 23.89.

C_{60}–Dithiapyrene dyad 4: C_{60} (190 mg, 0.26 mmol) was heated to reflux in toluene (80 mL). Compound **2** (35 mg, 0.13 mmol) and sarcosine (30 mg, 0.34 mmol) were added and the mixture was refluxed for 40 h. The solvent was removed in vacuo and the residue was purified by chromatography (silica, CS_2 + 2% Et_3N) to afford adduct **4** (85 mg, 64%) as a black powder. ^{1}H NMR (700 MHz, C_6D_6): δ = 5.94 (d, J=7.7 Hz, 1H), 5.55 (d, J=7.9 Hz, 1H), 5.46 (d, J=10.3 Hz, 1H), 5.28 (d, J=10.1 Hz, 1H), 5.02 (d, J=10.1 Hz, 1H), 4.97 (d, J=10.1 Hz, 1H), 4.93 (s, 1H), 4.35 (d, J=9.5 Hz, 1H), 4.26 (s, 1H), 3.75 (d, J=9.3 Hz, 1H), 2.40 ppm (s, 3H); MALDI-TOF MS: m/z: 1015 $[M]^+$; solubility of **4** was too low to produce an accurate ^{13}C NMR spectrum; elemental analysis calcd (%) for $C_{77}H_{13}NS_2$ (1016.06): C 91.02, H 1.29, N 1.38; S, 6.31; found C 91.08, H 1.34, N 1.32, S 6.26; UV/Vis (CH_2Cl_2): λ_{max} = 256, 305 sh, 322 sh, 394, 404 sh, 430, 704 nm.

C_{60}–pyrene dyad 6: C_{60} (625 mg, 0.87 mmol) was heated to reflux in chlorobenzene (200 mL). Pyrene-1-carboxaldehyde (**5**) (100 mg, 0.43 mmol) and sarcosine (77 mg, 0.86 mmol) were added and the mixture was refluxed overnight. The solvent was removed in vacuo and the residue was purified by chromatography (silica, carbon disulfide). Solvent was evaporated from the product fraction and the product was dissolved in a small amount of CS_2. Hexane was added to this solution and the formed precipitate was filtered off, washed with hexane and dried to yield compound **6** (25 mg, 56%) as a black powder. ^{1}H NMR (500 MHz, [D$_4$]*o*-dichlorobenzene + CS_2 (=10%) + trace C_6H_6): δ = 9.01 (d, J=9.3 Hz, 1H), 8.85 (d, J=7.9 Hz, 1H), 8.35 (d, J=9.7 Hz, 1H), 8.14–7.95 (m, 6H), 6.23 (s, 1H), 5.14 (d, J=9.6 Hz, 1H), 4.54 (d, J=9.2 Hz, 1H), 2.91 ppm (s, 3H). Due to restricted rotation around the exocyclic C–C bond between the pyrrolidine ring and the bulky pyrene ring, two thermodynamically stable (at ambient conditions) rotamers are possible for dyad **6**, which according to DFT calculations are of similar energies (Supporting Information, Figures S30, S31). They are formed in a ratio of ca 10:1 and are not separable by column chromatography. The second rotamer is clearly visible in the ^{1}H NMR spectrum as minor signals: δ = 10.56 (d, J=8.1 Hz, 1H), 8.32 (d, J=9.4 Hz, 1H), 8.24 (d, J=8.2 Hz, 1H), 8.20–8.17 (m, 2H), 8.14–7.95 (m, 4H), 5.71 (s, 1H), 5.18 (d, J=9.4 Hz, 1H), 4.37 (d, J=9.5 Hz, 1H), 2.96 ppm (s, 3H). ^{13}C NMR (125 MHz, d-ODCB + CS_2 + trace C_6H_6): δ = 156.8, 154.22, 154.15, 153.8, 147.5, 147.1, 146.9, 146.5, 146.42, 146.37, 146.3, 146.2, 146.1, 145.9, 145.84, 145.76, 145.72, 145.69, 145.6, 145.5, 145.40, 145.39, 145.3, 144.9, 144.7, 144.6, 144.5, 143.3, 143.2, 142.9, 142.8, 142.69, 142.68, 142.59, 142.56, 142.5, 142.4, 142.23, 142.18, 142.1, 142.0, 141.9, 141.72, 141.65, 140.6, 140.5, 139.8, 137.0, 136.8, 136.2, 136.0, 131.7, 131.4, 131.1, 128.3, 126.5, 126.0, 125.7, 125.5, 125.3, 123.7, 78.7, 70.5, 69.8, 40.4 ppm; ESI-MS: m/z: 976.1 $[M-H]^+$.

Cyclic voltammetry: Electrochemical experiments in benzonitrile (PhCN), *o*-dichlorobenzene (*o*-DCB) and their 1:1 v/v mixture were carried out using a BAS-CV50W electrochemical workstation with positive feedback compensation. Cyclic voltammetry was performed in a three-electrode cell equipped with a platinum disk (∅ 1.6 or 1.0 mm) as working electrode, platinum wire as a counter electrode and a non-aqueous Ag/Ag^+ reference electrode (0.01 M $AgNO_3$ in dry MeCN). The potential of the reference electrode was checked against the ferrocene/ferricinium couple (Fc/Fc^+) before and after each experiment, which showed the following average potentials against the reference electrode: +0.201 V (vs. Ag/Ag^+ in PhCN), +0.243 V (vs. Ag/Ag^+ in PhCN/*o*-DCB, 1:1 v/v), and the values of potentials were then re-calculated versus Fc/Fc^+ couple. Tetra-*n*-butylammonium hexafluorophosphate (Bu_4NPF_6) was used as supporting electrolyte and all experiments were performed under an argon atmosphere.

Pulse radiolysis: The pulse radiolysis experiments were performed by utilizing either 500 ns pulses of 1.55 MeV electrons or about 100 ns pulses of 3.8 V electrons from two different Van de Graff accelerator facilities. Details of the equipment and the analysis of data have been described elsewhere.[30]

Laser flash photolysis: Femtosecond transient absorption studies were performed with 387 nm laser pulses (1 kHz, 150 fs pulse width) from an amplified Ti/sapphire laser system (Clark-MXR, Inc.). For all photophysical experiments an error of 10% must be considered. Fluorescence spectra were recorded with a FluoroMax. The experiments were performed at room temperature. Each spectrum was an average of at least five individual scans and the appropriate corrections were applied. Pulse radiolysis experiments were accomplished using 50 ns pulses of 8 MeV electrons from a Model TB-8/16-1S electron linear accelerator. Nanosecond transi-

ent absorption measurements were carried out using a Nd/YAG laser (Continuum, SLII-10, 4–6 ns fwhm) at 355 nm with the power of 10 mJ as an excitation source. Photoinduced events were estimated by using a continuous Xe lamp (150 W) and an InGaAs–PIN photodiode (Hamamatsu 2949) as a probe light and a detector, respectively. The output from the photodiodes and a photomultiplier tube was recorded with a digitizing oscilloscope (Tektronix, TDS3032, 300 MHz). The transient spectra were recorded using fresh solutions in each laser excitation. All experiments were performed at 298 K.

Fluorescence: Fluorescence spectra were measured on a Shimadzu spectrofluorophotometer (RF-5000). The excitation wavelength was 422 nm in PhCN. The monitoring wavelength was corresponding to the maximum of the emission band at $\lambda_{max}=435$ nm. Typically, a PhCN solution (3.0 mL) was deaerated by argon purging for 8 min prior to the measurements.

Theoretical calculations: The ab initio computations for compounds **1**, **3**, and C_{60} were carried out with the Gaussian 03[31] package of programs at density-functional theory (DFT) level. The geometries were optimized using Pople's 6-31G split valence basis set supplemented by d polarization functions on heavy atoms. In the DFT calculations Becke's three-parameter hybrid exchange functional[32] with Lee–Yang–Parr gradient-corrected correlation functional (B3LYP)[33] were employed. No symmetry restrictions and no constraints of bonds/angles/dihedral angles were applied and all atoms were free to optimize. Electronic structures were calculated at the same B3LYP/6-31G(d) level of theory. Contours of HOMO and LUMO orbitals were visualized using Molekel v.4.3 program.[34]

Acknowledgements

This work was partially supported by a Grant-in-Aid for Scientific Research Priority Area (No. 19205019) from the Ministry of Education, Culture, Sports, Science and Technology, Japan and by the Office of Basic Energy Sciences of the US Department of Energy. We thank the ESF Eurocores SONS program NANOSYN and EPSRC for funding the work in Durham. This is document NDRL-5000 from the Notre Dame Radiation Laboratory.

[1] D. Gust, T. A. Moore, A. L. Moore, in *Electron Transfer in Chemistry, Vol. 3* (Ed.: V. Balzani), Wiley-VCH, Weinheim, **2001**, pp. 272–336.

[2] S. Fukuzumi, D. M. Guldi, in *Electron Transfer in Chemistry, Vol. 2* (Ed.: V. Balzani), Wiley-VCH, Weinheim, **2001**, pp. 270–337.

[3] D. M. Guldi, S. Fukuzumi, The Small Reorganization Energy of Fullerenes, in *Fullerenes: From Synthesis to Optoelectronic Properties* (Eds: D. M. Guldi, N. Martín), Kluwer, Dordrecht, **2003**, pp. 237–265.

[4] D. M. Guldi, P. V. Kamat, in: *Fullerenes, Chemistry, Physics, and Technology* (Eds.: K. M. Kadish, R. S. Ruoff), Wiley-Interscience, New York, **2000**, pp. 225–281.

[5] D. M. Guldi, *Chem. Commun.* **2000**, 321.

[6] a) T. Hasobe, H. Imahori, P. V. Kamat, T. K. Ahn, D. Kim, T. Hanada, T. Hirakawa, S. Fukuzumi, *J. Am. Chem. Soc.* **2005**, *127*, 1216; b) T. Hasobe, P. V. Kamat, V. Troiani, N. Solladié, T. K. Ahn, S. K. Kim, D. Kim, A. Kongkanand, S. Kuwabata, S. Fukuzumi, *J. Phys. Chem. B* **2005**, *109*, 19.

[7] T. Hasobe, S. Fukuzumi, P. V. Kamat, *Interface* **2006**, *15*, 47.

[8] S. Fukuzumi, in *The Porphyrin Handbook, Vol. 8* (Eds.: K. M. Kadish, K. M. Smith, R. Guilard), Academic Press, San Diego, **2000**, pp. 115–151.

[9] S. Fukuzumi, H. Imahori, in *Electron Transfer in Chemistry, Vol. 2* (Ed.: V. Balzani), Wiley-VCH, Weinheim, **2001**, pp. 927–975.

[10] a) M. R. Wasielewski, in *Photoinduced Electron Transfer* (Eds.: M. A. Fox, M. Chanon), Elsevier, Amsterdam, **1988**, Part A, pp. 161–206; b) M. R. Wasielewski, *Chem. Rev.* **1992**, *92*, 435.

[11] H. Imahori, M. E. El-Khouly, M. Fujitsuka, O. Ito, Y. Sakata, S. Fukuzumi, *J. Phys. Chem. A* **2001**, *105*, 325.

[12] M. Bendikov, F. Wudl, D. F. Perepichka, *Chem. Rev.* **2004**, *104*, 4891.

[13] a) E. Allard, J. Cousseau, J. Ordúna, J. Garín, H. Luo, Y. Araki, O. Ito, *Phys. Chem. Chem. Phys.* **2002**, *4*, 5944; b) S. Chopin, Z. Gan, J. Cousseau, Y. Araki, O. Ito, *J. Mater. Chem.* **2005**, *15*, 2288.

[14] M. D. Valentin, A. Bisol, G. Agostini, P. A. Liddell, G. Kodis, A. L. Moore, T. A. Moore, D. Gust, D. Carbonera, *J. Phys. Chem. B* **2005**, *109*, 14401.

[15] a) N. Martín, L. Sánchez, C. Seoane, R. Andreu, J. Garín, J. Orduna, *Tetrahedron Lett.* **1996**, *37*, 5979; b) N. Martín, L. Sánchez, M. A. Herranz, D. M. Guldi, *J. Phys. Chem. A* **2000**, *104*, 4648; c) D. M. Guldi, S. González, N. Martín, A. Antón, J. Garín, J. Orduna, *J. Org. Chem.* **2000**, *65*, 1978.

[16] a) J. L. Segura, E. M. Priego, N. Martín, *Tetrahedron Lett.* **2000**, *41*, 7737; b) A. G. Burly, A. G. Avent, O. B. Boltina, V. G. Ilya, D. M. Guldi, M. Marrcaccio, F. Paolucci, D. Paolucci, R. Taylor, *Chem. Commun.* **2003**, 148.

[17] K. Nakasuji, J. Toyoda, K. Imaeda, H. Inokuchi, I. Murata, A. Oda, A. Kawamoto, J. Tanaka, *Synth. Met.* **1991**, *42*, 2529.

[18] K. Nakasuji, H. Kubata, T. Kotani, I. Murata, G. Saito, T. Enoki, K. Imaeda, H. Inokuchi, M. Honda, C. Katayama, J. Tanaka, *J. Am. Chem. Soc.* **1986**, *108*, 3460.

[19] Y. Morita, E. Miyazaki, J. Toyoda, K. Nakasuji, *Bull. Chem. Soc. Jpn.* **2003**, *76*, 205.

[20] Y. Morita, E. Miyazaki, J. Kawai, K. Sato, D. Shiomi, T. Takui, K. Nakasuji, *Polyhedron* **2003**, *22*, 2219.

[21] a) Y. Morita, E. Miyazaki, H. Yamochi, G. Saito, K. Nakasuji, *Synth. Met.* **2003**, *135–136*, 581; b) E. Miyazaki, Y. Morita, K. Nakasuji, *Polyhedron* **2005**, *24*, 2632.

[22] R. Dennington II, T. Keith, J. Millam, K. Eppinnett, W. L. Hovell, R. Gilliland, Semichem, Inc., Shawnee Mission, KS (USA), **2003**.

[23] M. Eiermann, R. G. Hicks, B. W. Knight, H. Neugebauer, F. Wudl, *Electrochem. Soc. Proceedings* **2004**, *22*, 407.

[24] F. Giacalone, J. L. Segura, N. Martín, J. Ramey, D. M. Guldi, *Chem. Eur. J.* **2005**, *11*, 4819.

[25] H. Imahori, K. Tamaki, D. M. Guldi, C. Luo, M. Fujitsuka, O. Ito, Y. Sakata, S. Fukuzumi, *J. Am. Chem. Soc.* **2001**, *123*, 2607.

[26] A. S. D. Ssandanayaka, Y. Araki, O. Ito, G. R. Deviprasad, P. M. Smith, L. M. Rogers, M. E. Zandler, F. D′Souza, *Chem. Phys.* **2006**, *325*, 452.

[27] a) R. A. Marcus, *Annu. Rev. Phys. Chem.* **1964**, *15*, 155; b) R. A. Marcus, N. Sutin, *Biochim. Biophys. Acta* **1985**, *811*, 265; c) R. A. Marcus, *Angew. Chem.* **1993**, *105*, 1161; *Angew. Chem. Int. Ed. Engl.* **1993**, *32*, 1111.

[28] M. Maggini, G. Scorrano, M. Prato, *J. Am. Chem. Soc.* **1993**, *115*, 9798.

[29] C. K. Mann, K. K. Barnes, in *Electrochemical Reaction in Nonaqueous Systems*, Marcel Dekker, New York, **1970**.

[30] E. Janata, *Radiat. Phys. Chem.* **1992**, *40*, 437.

[31] Gaussian 03, Revision B.04, M. J. Frisch, G. W. Trucks, H. B. Schlegel, G. E. Scuseria, M. A. Robb, J. R. Cheeseman, J. A. Montgomery, Jr., T. Vreven, K. N. Kudin, J. C. Burant, J. M. Millam, S. S. Iyengar, J. Tomasi, V. Barone, B. Mennucci, M. Cossi, G. Scalmani, N. Rega, G. A. Petersson, H. Nakatsuji, M. Hada, M. Ehara, K. Toyota, R. Fukuda, J. Hasegawa, M. Ishida, T. Nakajima, Y. Honda, O. Kitao, H. Nakai, M. Klene, X. Li, J. E. Knox, H. P. Hratchian, J. B. Cross, V. Bakken, C. Adamo, J. Jaramillo, R. Gomperts, R. E. Stratmann, O. Yazyev, A. J. Austin, R. Cammi, C. Pomelli, J. W. Ochterski, P. Y. Ayala, K. Morokuma, G. A. Voth, P. Salvador, J. J. Dannenberg, V. G. Zakrzewski, S. Dapprich, A. D. Daniels, M. C. Strain, O. Farkas, D. K. Malick, A. D. Rabuck, K. Raghavachari, J. B. Foresman, J. V. Ortiz, Q. Cui, A. G. Baboul, S. Clifford, J. Cioslowski, B. B. Stefanov, G. Liu, A. Liashenko, P. Piskorz, I. Komaromi, R. L. Martin, D. J. Fox, T. Keith, M. A. Al-Laham, C. Y. Peng, A. Nanayakkara, M. Challacombe, P. M. W. Gill, B. Johnson, W. Chen, M. W. Wong, C. Gonzalez, J. A. Pople, Gaussian, Inc., Wallingford CT, **2004**.

[32] A. D. Becke, *Phys. Rev. A* **1988**, *38*, 3098; A. D. Becke, *J. Chem. Phys.* **1993**, *98*, 5648.
[33] C. Lee, W. Yang, R. G. Parr, *Phys. Rev. B* **1988**, *37*, 785.
[34] a) P. Flükiger, H. P. Lüthi, S. Portmann, J. Weber, Molekel, Version 4.3, Swiss Center for Scientific Computing, Manno (Switzerland), **2002**; http://www.cscs.ch/molekel/; b) S. Portmann, H. P. Lüthi, *Chimia* **2000**, *54*, 766.

Received: June 2, 2007
Published online: September 28, 2007

